ISSN:2790-1688 Volume-15-(2025)

Navigation and Bearing-only Cascade Formation Control for Robots Using Panel and Leader-Follower Method

Qing Han [1, &], Biao He [1, &], Jinping Chen [2, *, &], Haochuan Wan [1, &], Jianxiong Zhang [1, &]

[1] School of Robot Engineering, Yangtze Normal University, Fuling 408100, Chongqing, China;

[2] School of Mechanical Engineering, Zhengzhou University of Aeronautics, Zhengzhou 450046,China.

[&] These authors contributed equally to this work

Abstract. This paper proposes an autonomous navigation method for a leader robot based on the panel method. Bearing-only cascade formation control for robots are achieved using a leader-follower approach and is found to be effective in complex obstacle environments, which is a single-directional cascade structure for multi-robot queuing. In this formation, each robot serves as both a follower to its predecessor and a leader to its successor, with intermediate robots simultaneously fulfilling both roles. The follower robots are constrained to only perceive the bearing information of their immediate leader. To demonstrate the proposed method, a collision-free path is first planned for the leader robot using the panel method along the streamline direction from the point of departure to the ending point. Next, a cascade multi-robot formation in a complex obstacle environment is established using the leader-follower method. Finally, the effectiveness and feasibility of the leader robot and multi-robot formations are verified through simulation.

Keywords: Autonomous navigation method; Panel method; Pure angle observation information; Cascade multi-robot formation.

1. Introduction

Multi-robot systems are widely used in many fields including service robotics [1], agriculture [2], oil and gas exploration [3], aerospace [4], medicine [5], surveillance [6]. In these applications, multiple robots perform tasks that are either very difficult or impossible for a singular robot to accomplish. Multi-robot configurations have garnered significant interest across academic, industrial, and corporate circles in recent decades.

Systems composed of multiple robots have better flexibility, adaptability, and robustness compared to single-robot systems [7]. However, creating and maintaining multi-robot formations are highly challenging when working within cluttered environments. There are three main approaches to formation control: leader-follower methods, virtual structure methods, and behaviour-based methods. Among these, leader-follower methods [8-12] stand out for their simplicity, scalability, flexibility, adaptability, and reliability; they are widely used throughout many fields, so the cascade formation control problem is studied in [9-13], which is hot topic about multiple robots formation control.

The “leader” robot plays a crucial role in cascade multi-robot formations using leader-follower control. A collision-free path must be planned carefully for the leader to achieve the desired formation; this can be achieved through the panel method, moving along the streamline direction from the point of departure to the ending point in cluttered static or dynamic environments. In these cases, arbitrarily shaped obstacles have no impact on the path of the leader robot. The panel method is a robust numerical approach to solving potential flow problems around the boundaries of arbitrarily shaped obstacles. It can be used to more effectively manage complex objects compared to other algorithms due to its simplicity, speed, and accuracy. It has been utilized extensively for path planning [14-16] and navigation [17-22], allowing for analytical solutions to flowlines in environments with multiple complex obstacles that are often impossible to solve analytically. When

applied to mobile robots [14], the panel method can guarantee the desired motion is achieved in partially unknown static and dynamic environments based on the automatic adjustment of potential field parameters. The panel method has also been improved in terms of robustness for path planning in environments with moving obstacles [15], and to plan guide paths for underwater gliders [16] for enhanced reliability and efficiency.

The panel method has also been used for safe swarm-robot navigation [17-22]. The panel method has been used for safe swarm-robot navigation enabling robots to maintain predefined geometric formations by following streamlines and using potential functions [17]. Safe paths between the robots and the target can be planned in real-time using this method, while maintaining the desired formation of multiple robots from the point of departure to the end point based on potential functions [18]. Artificial potential functions can be further utilized to accomplish this with a formation of predefined geometrical shapes [19]. In maritime contexts, the 3D Rankine panel method has been used to solve seakeeping problems for ultra large container ships operating amidst asymmetric regular waves [20]. The 2D panel method can be used to calculate lift and pitching moment coefficients efficiently and with relatively little computational burden [21]. A panel-method-based guidance algorithm was developed for real-time path planning in urban environments, offering efficient navigation for multiple vehicles [22]. In [17-19], the panel method has been used for safe multiple robots navigation paths, while maintaining the desired formation of multiple robots based on potential functions, and thus inevitably leads to local minima problems during navigation by using artificial potentials. In this study, the panel method and leader-follower method were applied to achieve collision-free navigation for a leader robot and to maintain cascade multi-robot formations， respectively. Once the leader robot establishes a collision-free path, follower robots can quickly form and sustain a desired configuration. This effectively avoids local minima problems during navigation by using artificial potentials [5], [17-19].

The contributions of this work are threefold. First, a collision-free path is established for the leader robot using the panel method, moving along the streamline direction from the point of departure to the end point. Second, based on this path, the leader-follower strategy is enacted during navigation so that multiple robots can swiftly fall into and maintain a cascade desired formation. Third, simulation results demonstrate the effectivenesses of the proposed approach in efficiently guiding leader robots to targets and in maintaining designated cascade multi-robot formations.

The remainder of this paper is organized as follows: Section 2 presents a collision-avoidance navigation path for the leader robot, determined based on the panel method. Section 3 presents the least squares fitting method for irregularly shaped obstacles using circles or arcs, and Section 4 presents “1-1-1” cascade leader-follower multi-robot formation control. Section 5 reports simulation results that validate the proposed method. Section 6 provides a brief summary and concluding remarks

2. Organization of the Text

2.1 Panel-method-based collision avoidance for leader robots

The panel method is employed in this study to solve the potential flow problem around rigid bodies, thus planning a collision-free path for a leader robot in cluttered static and dynamic environments. This method allows for path planning along the streamline direction from the point of departure to the end point, effectively avoiding objects with complex, rigid shapes. According to a previously established theory of the panel method [23,24], the linear velocities of the leader robot at each position can be computed to enable the planning of a collision-free path from the starting point to the target.

When a rigid body is submerged in a fluid, the flow cannot penetrate its surface and remains tangent to its boundaries. The body can be discretized into small panels to which flow singularity

elements are individually assigned. The normal component of the relative velocity at the boundary between the fluid and the solid surface is zero under these conditions, which can be expressed mathematically as follows:

$$\vec{\mathbf{V}}\cdot\vec{\mathbf{n}}=0 \tag{1}$$

where $\vec{\mathbf{V}}$ is the relative velocity of the fluid, and $\vec{\mathbf{n}}$ is the surface normal [23].

The potential flow model used for robot navigation has a velocity composed of four main components: the induced velocity $\vec{\mathbf{V}}_{induce}^{j}$ caused by the presence of obstacles, the free stream velocity $\vec{\mathbf{V}}_{infree}$, the source velocity $\vec{\mathbf{V}}_{source}$ resulting from the effects of the source point, and the sink velocity $\vec{\mathbf{V}}_{sink}$ owing to a sink situated at the target which attracts and absorbs streamlines. Dividing the surface of the complex rigid obstacle surface into *N* panels shifts the boundary condition to:

$$\left(\sum_{j=1}^{N}\vec{\mathbf{V}}_{induce}^{j}+\vec{\mathbf{V}}_{infree}+\vec{\mathbf{V}}_{source}+\vec{\mathbf{V}}_{sink}\right)\cdot\vec{\mathbf{n}}=0 \tag{2}$$

Shifting known parameters the right-hand side of Eq. (2) yields Eq. (3):

$$\sum_{j=1}^{N}\vec{\mathbf{V}}_{induce}^{j}\cdot\vec{\mathbf{n}}=\sum_{j=1}^{N}\vec{q}^{\,j}=-\left(\vec{\mathbf{V}}_{infree}+\vec{\mathbf{V}}_{source}+\vec{\mathbf{V}}_{sink}\right)\cdot\vec{\mathbf{n}}=RHS \tag{3}$$

The velocity at a point (*x*, *y*) in the space can be expressed as Eq. (4), owing to the induction by a vortex point with strength Γ_j located at (x_j, y_j) in panel *j*:

$$\vec{\mathbf{V}}_{induce}^{j}=\left(v_{x\_induce}^{j},v_{y\_induce}^{j}\right)=\frac{\Gamma_j}{2\pi\left[\left(x-x_j\right)^2+\left(y-y_j\right)^2\right]}\left(\left(y-y_j\right),-\left(x-x_j\right)\right) \tag{4}$$

where $v_{x\_induce}^{j}$ and $v_{y\_induce}^{j}$ are the components of the induced velocity along the x-axis and y-axis, respectively.

Similarly, the velocity at a point *(x, y)* in space can be expressed as Eq. (5), owing to a source with strength Γ_{source} located at (x_{source}, y_{source}):

$$\vec{\mathbf{V}}_{source}=\left(v_{x\_source},v_{y\_source}\right)=\frac{\Gamma_{source}}{2\pi\left[\left(x-x_{source}\right)^2+\left(y-y_{source}\right)^2\right]}\left(\left(x-x_{source}\right),\left(y-y_{source}\right)\right) \tag{5}$$

where v_{x_source} and v_{y_source} are the components of the source velocity along the x-axis and y-axis, respectively. Analogously, the velocity at a point *(x, y)* in the space can be expressed by Eq. (6), owing to a sink with strength $\Gamma_{\sin k}$ at location $(x_{\sin k}, y_{\sin k})$:

$$\vec{\mathbf{V}}_{sink}=\left(v_{x\_sink},v_{y\_sink}\right)=\frac{-\Gamma_{sink}}{2\pi\left[\left(x-x_{sink}\right)^2+\left(y-y_{sink}\right)^2\right]}\left(\left(x-x_{sink}\right),\left(y-y_{sink}\right)\right) \tag{6}$$

where $x_{\sin k}$ and v_{y_sink} are the components of the sink velocity along the x-axis and y-axis, respectively.

The influence factor a_{ij} describes the "induction ability," or the orthogonal velocity to the surface of the rigid body. Accordingly, the influence factor a_{1j} at point (x_1, y_1) in space generated by the singularity element with unit strength ($\Gamma_j=1$) at (x_j, y_j) can be defined as:

$$a_{1j}=\left(v_{x\_induce},\ v_{y\_induce}\right)_{1j}\cdot\mathbf{n}_1 \tag{7}$$

The orthogonal velocity at the initial point (x_1, y_1) corresponding to all the singularity elements of *N* panels is given by:

$$(q)_{1N}=a_{11}\Gamma_1+a_{12}\Gamma_2+\cdots+a_{1N}\Gamma_N \tag{8}$$

where $(\Gamma_1\cdots\Gamma_N)$ are the unknown parameters. According to Eqs. (3) and (8), the tangency boundary condition at point (x_1, y_1) is thus:

$$\begin{aligned}&\left(a_{11}\Gamma_1+a_{12}\Gamma_2+\cdots+a_{1N}\Gamma_N\right)=RHS_1=\\&-\left(\left(v_{x\_infree},v_{y\_infree}\right).\mathbf{n}_1+\left(v_{x\_source},v_{y\_source}\right).\mathbf{n}_1+\left(v_{x\_sink},v_{y\_sink}\right).\mathbf{n}_1\right)\end{aligned} \tag{9}$$

Analogously, the boundary conditions of N points can be defined as:

$$\begin{pmatrix}a_{11}&a_{12}&\cdots&a_{1N}\\a_{21}&a_{22}&\cdots&a_{2N}\\\vdots&\vdots&\cdots&\vdots\\a_{N1}&a_{N2}&\cdots&a_{NN}\end{pmatrix}\begin{pmatrix}\Gamma_1\\\Gamma_2\\\vdots\\\Gamma_N\end{pmatrix}=\begin{pmatrix}RHS_1\\RHS_2\\\vdots\\RHS_N\end{pmatrix} \tag{10}$$

The parameters $\begin{pmatrix}\Gamma_1&\Gamma_2&\cdots&\Gamma_N\end{pmatrix}$ can be calculated using Eq. (10). The speed of the robot at each position on a collision-free path from the point of departure towards the end point is given by:

$$\begin{bmatrix}\mathbf{V}_{x\_robot}\\\mathbf{V}_{y\_robot}\end{bmatrix}=\begin{bmatrix}v_{x\_infree}+v_{x\_source}+v_{x\_sink}+\sum_{j=1}^{N}\left(v_{x\_induce}\right)_j\\v_{y\_infree}+v_{y\_source}+v_{y\_sink}+\sum_{j=1}^{N}\left(v_{y\_induce}\right)_j\end{bmatrix} \tag{11}$$

The boundary condition and panel method are used here to identify streamlines. The calculations focus on the boundaries of rigid objects rather than the entire flow field, which lends simplicity and efficiency in planning navigation paths for the robot. Discretizing the rigid obstacle surface with more panels improves the accuracy of the results, however, which causes a corresponding increase in the computational cost.

2.2 Least squares fitting method for irregularly shaped obstacles with circles or arcs

A previously proposed least squares method [25] was applied in this study to regularize irregular obstacles and achieve autonomous navigation of the robot in environments containing complex obstacles. First, discrete points on the surfaces of rigid obstacles were selected. Next, a circle or arc was fitted based on the least squares method. Finally, a safe and collision-free path for the robot was determined based on the panel method.

The least squares method for fitting a circle or arc is based on the minimum root mean square distance from the circle or arc to a discrete point, where $\left(x_j,y_j\right)$ are the coordinates of n discrete points. The objective function is:

$$f=\sum_{j=1}^{n}d_j^2 \tag{12}$$

where $1\le j\le n$, and d_j is the Euclidean distance from discrete points to points on the fitted circle or arc. The expression for fitting a circle is:

$$\left(x-m\right)^2+\left(y-n\right)^2=R^2 \tag{13}$$

where (m,n) is the center of the fitted circle and R is its radius. After determining the center and radius of the fitted circle, d_j can be computed as:

$$d_j=\left|\sqrt{\left(x_j-m\right)^2+\left(y_j-n\right)^2}-R\right| \tag{14}$$

There is currently no simple and effective least squares algorithm that can directly solve for circle or arc fitting in a closed form. Solving the minimum value of the objective function f in Eq. (12) is a nonlinear problem to which no analytical solution is tractable, so an approximation is appropriate.

As depicted in Fig. 1， the least squares method used in a previous study [25] was applied for the robot navigation task. First, ten discrete points (marked in red) on the surface of the rigid obstacle were selected to fit a segment of an arc. Next, the arc was discretized into 10 panels. Finally, a vortex point (marked in light green) and a collection point (marked in black) were selected at a quarter of each panel and at three quarters of each panel, respectively.

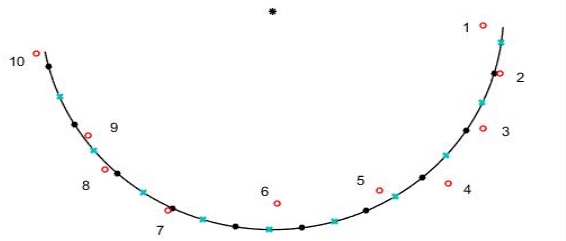

Figure 1: Least squares fitting method using circles or arcs

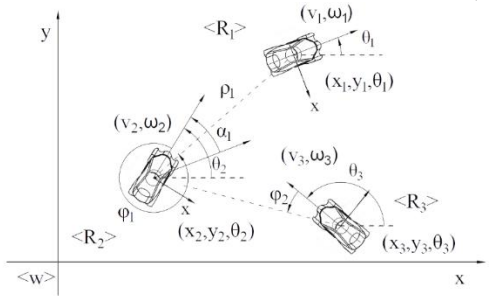

Figure 2: Leader-follower coordinate representation

2.3 “1-1-1” cascade leader-follower multi-robot formation control

The strengths of vortex elements can be calculated according to the boundary conditions in Eq. (10), then so can the velocity of the robot at any coordinate along the streamline direction in the environment. Because the streamlines navigate around obstacles without intersecting them, the robot can safely avoid collisions from the point of departure towards the end point along the streamline direction. When the leader robot follows a safe and collision-free path, the full cascade multi-robot formation can navigate the environment effectively via the leader-follower method.

2.3.1 Kinematics model of "1-1-1" cascade leader-follower robot formation

In the hierarchical formation control framework illustrated in Figure 1, a cascade leader-follower structure is established where R1 leads R2, which in turn leads R3. Each robot's control inputs consist of its linear velocity (vi) and angular velocity (ωi), (i=1,2,3). ρ_i is the inter-robot distance between consecutive robots' centroids, φ_i is the bearing angle measured from the follower's local y-axis to the leader's centroid. The absolute orientations of the leader (θ_i) and follower (θ_j) are both referenced to the global world frame $\langle \mathrm{W} \rangle$, with their orientation difference computed as $\alpha_i \triangleq \theta_i - \theta_j$.

Referring to the hierarchical formation control framework illustrated in Figure 2, the kinematic model governing the cascade leader-follower robot formation can be mathematically described by equation (15),

$$S_n : \begin{cases} \dot{\boldsymbol{s}} = f(s,u) = F(s)U \\ \boldsymbol{y} = h(s) = \left[h_1^{\mathrm{T}}(s), h_2^{\mathrm{T}}(s) \right]^{\mathrm{T}} \end{cases} \tag{15}$$

where state vector $\boldsymbol{s} \triangleq [s_1^{\mathrm{T}}, s_2^{\mathrm{T}}]^{\mathrm{T}}$, $\boldsymbol{s}_1 \triangleq [\rho_1 \quad \varphi_1 \quad \alpha_1]^{\mathrm{T}}$, $\boldsymbol{s}_2 \triangleq [\rho_2 \quad \varphi_2 \quad \alpha_2]^{\mathrm{T}}$, $\delta_i = \varphi_i + \alpha_i \ (i = 1,2)$, input vector $\boldsymbol{U} \triangleq [v_1 \quad \omega_1 \quad v_2 \quad \omega_2 \quad v_3 \quad \omega_3]^{\mathrm{T}}$, output vector $\boldsymbol{y} = h(s) = \left[h_1^{\mathrm{T}}(s), h_2^{\mathrm{T}}(s) \right]^{\mathrm{T}}$, $h_1 \triangleq [\varphi_1 \quad \alpha_1]^{\mathrm{T}}$, $h_2 \triangleq [\varphi_2 \quad \alpha_2]^{\mathrm{T}}$,

$$\dot{s} = \begin{bmatrix} \dot{\rho}_1 \\ \dot{\varphi}_1 \\ \dot{\alpha}_1 \\ \dot{\rho}_2 \\ \dot{\varphi}_2 \\ \dot{\alpha}_2 \end{bmatrix} = F(s)U = \begin{bmatrix} v_1 \cos\delta_1 - v_2 \cos\varphi_1 \\ -v_1 \sin\delta_1 / \rho_1 + v_2 \sin\varphi_1 / \rho_1 - \omega_2 \\ \omega_1 - \omega_2 \\ v_2 \cos\delta_2 - v_3 \cos\varphi_2 \\ -v_2 \sin\delta_2 / \rho_2 + v_3 \sin\varphi_2 / \rho_2 - \omega_3 \\ \omega_2 - \omega_3 \end{bmatrix} = \begin{bmatrix} \cos\delta_1 & 0 & -\cos\varphi_1 & 0 & 0 & 0 \\ -\sin\delta_1 / \rho_1 & 0 & \sin\varphi_1 / \rho_1 & -1 & 0 & 0 \\ 0 & 1 & 0 & -1 & 0 & 0 \\ 0 & 0 & \cos\delta_2 & 0 & -\cos\varphi_2 & 0 \\ 0 & 0 & -\sin\delta_2 / \rho_2 & 0 & \sin\varphi_2 / \rho_2 & -1 \\ 0 & 0 & 0 & 1 & 0 & -1 \end{bmatrix} \begin{bmatrix} v_1 \\ \omega_1 \\ v_2 \\ \omega_2 \\ v_3 \\ \omega_3 \end{bmatrix}$$

Building upon the previously established single-stage formation model (Equation 15), the kinematic framework for multistage cascade leader-follower formations can be systematically derived through a straightforward extension.

$$S_n : \begin{cases} \dot{\boldsymbol{s}} = f(s,u) = \left[f_1^{\mathrm{T}}(s_1, u_1), \quad \ldots, \quad f_{n+1}^{\mathrm{T}}(s_n, u_{n+1}) \right]^{\mathrm{T}} \\ \boldsymbol{y} = h(s) = \left[h_1^{\mathrm{T}}(s_1), \quad \ldots, \quad h_n^{\mathrm{T}}(s_n) \right]^{\mathrm{T}} \end{cases} \tag{16}$$

where $\boldsymbol{s} = \left[s_1^{\mathrm{T}}, s_2^{\mathrm{T}}, \cdots, s_n^{\mathrm{T}} \right]^{\mathrm{T}} \in \mathbb{R}^{3n}$ is the state vector, $\boldsymbol{U} = \left[u_1^{\mathrm{T}}, u_2^{\mathrm{T}}, \cdots, u_{n+1}^{\mathrm{T}} \right]^{\mathrm{T}} \in \mathbb{R}^{2(n+1)}$ is the control input vector, $h : \mathbb{R}^{2n} \mapsto \mathbb{R}^{2n}$ and $f : \mathbb{R}^{3(n+1)} \times \Lambda \mapsto \mathbb{R}^{3(n+1)}$.

2.3.2 A bearing-only UKF-based input-output feedback control

To implement the feedback control architecture, state estimation is essential. In this work, we employ the Unscented Kalman Filter (UKF) to estimate the robots' states. By integrating the UKF algorithm with the input-output state feedback control framework, the formation control system can effectively utilize bearing-only measurements from the cascade robot formation to achieve motion control. This integration enables the realization of the desired cascade formation control objectives.

2.3.2.1 UKF Algorithm

For formation control purposes, an accurate estimation $\hat{s}$ of the true system state s is essential. Using the input vector U and the output vector $y = h(s) = \left[h_1^{\mathrm{T}}(s), \cdots, h_n^{\mathrm{T}}(s)\right]^{\mathrm{T}}$, the UKF in [26] is specifically designed to estimate angle information, which constitutes a critical component of the state vector, and we can integrate the Euler forward method with the UKF algorithm to obtain more precise state information. The process equation (17) and measurement equation (18) with additive noise can be modeled as follows:

$$\dot{s} = F(s)U + O \tag{17}$$

$$y = Gs + N \tag{18}$$

In this framework, G serves as the output transition matrix, while O and N represent zero-mean white Gaussian noise processes with covariance matrices P_L and P_N, respectively. These terms are assumed to be mutually uncorrelated. To derive the discrete-time representation, we apply the Euler forward method with sampling period T_c, discretizing equation (17) to yield equation (19).

$$s(k+1) = \Gamma(s(k), u(k)) + T_c O \tag{19}$$

where $\Gamma(s(k), u(k)) = T_c F(s)U + s(k)$.

As described in [26], the UKF operates through a two-step process: prediction and correction, based on the Unscented Transformation principle. To improve robot localization performance, both the process equation (17) and measurement equation (18) require proper sampling.

2.3.2.2 Input-Output State Feedback Control

The control law is specifically developed for robots R_1 and R_2, with an analogous design applied to all other robots in the cascade formation. By reformulating the state equation presented in (15), the first-level kinematic system model of the cascade formation can be equivalently expressed as equation (20). Further derivation of $\alpha_1 = \theta_1 - \theta_2$ then yields equation (21)

$$\dot{s}_r = A(s)U_1 + B(s)U_2 \tag{20}$$

$$\dot{\alpha}_1 = \omega_1 - \omega_2 \tag{21}$$

In this context, $s_r \triangleq [\rho_1 \quad \varphi_1]^{\mathrm{T}}$ represents the reduced state-space vector. Matrix $E(\mathrm{s})^{2\times4}$ corresponds to the upper-left submatrix of $F(\mathrm{s})$, while matrices $A(\mathrm{s})^{2\times2}$ matrices and $B(\mathrm{s})^{2\times2}$ correspond to the upper-left and right submatrices of $E(\mathrm{s})^{2\times4}$, respectively.

Leveraging standard input-output linearization techniques [27], we develop an input-output state feedback control strategy for robot formation control. Based on equation (20), the control input for R_2 is formulated as:

$$U_2 \triangleq [v_2 \quad \omega_2]^{\mathrm{T}} = B(s)^{-1}(C - A(s)U_1) \tag{22}$$

where $A(\mathrm{s}) = \begin{bmatrix} \cos\delta & 0 \\ -\sin\delta_1 / \rho_1 & 0 \end{bmatrix}$, $B(\mathrm{s}) = \begin{bmatrix} -\cos\varphi_1 & 0 \\ \sin\varphi_1 / \rho_1 & -1 \end{bmatrix}$, $C = -K(s_r - s_r^{\mathrm{ide}})$, $K = diag\left[k_1 \quad k_2\right]$, with $k_1, k_2 > 0$. The superscript "ide" denotes the desired state, while C serves as an auxiliary control parameter. Equation (22) acts in equation (20) as a feedback linearizing control. In conjunction with equation (21), this yields the closed-loop dynamics described by equation (23).

$$\begin{aligned} \dot{s}_r &= C = -K(s_r - s_r^{\mathrm{ide}}) = \begin{bmatrix} k_1(\rho_1^{\mathrm{ide}} - \rho_1) \\ k_2(\varphi_1^{\mathrm{ide}} - \varphi_1) \end{bmatrix} \\ \dot{\alpha}_1 &= \omega_1 - \omega_2 \end{aligned} \tag{23}$$

2.4 Simulations and experiments

The simulation results presented in this section validate the autonomous navigation capability of the leader robot, established based on the panel method, and the cascade multi-robot formation

control method discussed above. The simulation environment consists of three robots(R_2 following R_1, and R_3 following R_2). Simulations were carried out in MATLAB. The flow includes a source point, a sink point, and several vortex points. The source point produces a repulsive force on the robots, the sink point produces an attraction force on the robots, and the vortex point produces a vortex force on the robots. The leader robot navigates toward its target along the calculated streamline paths under the combined influence of these forces. The panel method yields a collision-free path that the leader robot traverses, enabling the cascade multi-robot formation to proceed through the environment safely via the leader-follower method.

2.4.1 Initial conditions

As shown in Fig. 3, the simulation environment includes the leader robot located at $(-20,-10)$ and two irregularly shaped rigid-body obstacles. The source point with (Γ_{source}=20 N) and sink point with (Γ_{sink}=40 N) are located at $(-40,-10)$ and $(60,60)$, respectively. Obstacle$_1$ and obstacle$_2$, are divided into 10 panels each. The panel strengths calculated according to Eq. (10) are shown in Table 1 and Table 2, respectively.

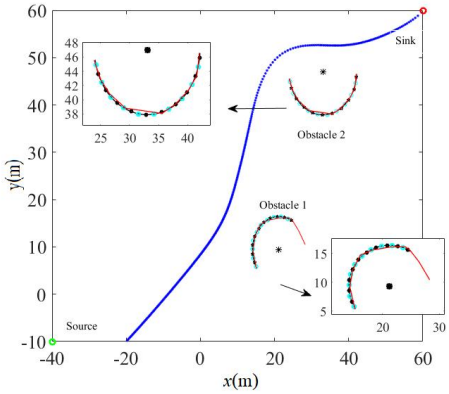

Figure 3: Navigation path of leader robot in formation obstacle environmen

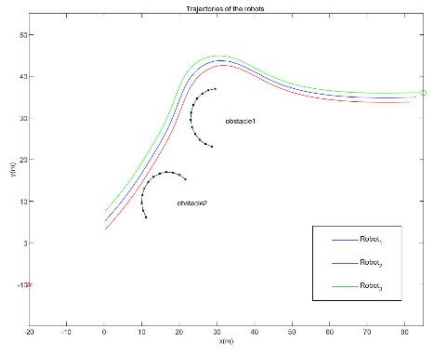

Figure 4: Trajectories of cascade multi-robot

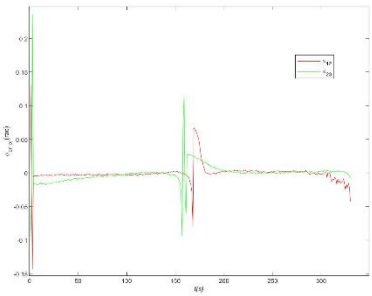

Figure 5: Observation angle estimation errors of robots

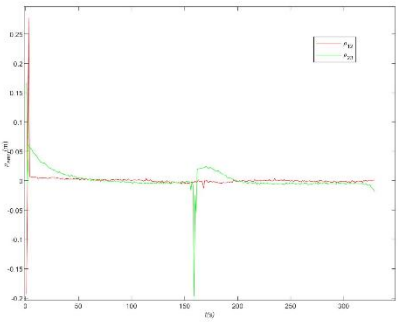

Figure 6: Distance errors of of robots

Table 1: Panel strength produced on Obstacle 1

panel number	strength value	panel number	strength value	panel number	strength value	panel number	strength value	panel number	strength value
1	-0.975	2	-2.474	3	-2.585	4	-3.036	5	4.365
6	-10.819	7	13.856	8	3.881	9	2.141	10	1.298

Table 2: Panel strength produced on Obstacle 2

panel number	strength value	panel number	strength value	panel number	strength value	panel number	strength value	panel number	strength value

1	2.665	2	1.045	3	0.741	4	0.653	5	0.742
6	-11.299	7	0.060	8	0.210	9	0.278	10	0.327

The initial configuration vectors for the leader robot and follower robots are specified as follows:

$$\begin{aligned}\left[x_1(0) \quad y_1(0) \quad \theta_1(0)\right]^{\mathrm{T}} &= [0 \quad 5.0 \quad \pi/5]^{\mathrm{T}} \\ \left[x_2(0) \quad y_2(0) \quad \theta_2(0)\right]^{\mathrm{T}} &= [0 \quad 3.0 \quad \pi/5]^{\mathrm{T}} \\ \left[x_3(0) \quad y_3(0) \quad \theta_3(0)\right]^{\mathrm{T}} &= [0 \quad 7.0 \quad \pi/5]^{\mathrm{T}}\end{aligned} \tag{24}$$

The key parameters for the UKF and the input-output state feedback control law are as follows:

It is assumed that $s_{r1}^{ideal} = [0.9 \quad 7\pi/4]$, $s_{r2}^{ideal} = [0.9 \quad 3\pi/2]$, and the units for distances and angles are millimeters and radians, respectively. The gains of the controller are $k_1 = 0.15$ and $k_2 = 0.25$. The other parameters of the UKF are $T_c = 0.01\mathrm{s}$, $\mathrm{P}_F = diag([h \quad h])$, $\mathrm{P}_G = diag([h \quad h])$, and $P = ([1.13 \quad 1.13])$, where $h = 3.0 \times 10^{-2}\ \mathrm{rad}^2$.

2.4.2 Simulation analysis

The irregular, rigid obstacles in the simulation environment are depicted in Figs. 3. Some points on the surface of these rigid obstacles were selected and connected to segmented straight lines; these lines were fitted using the curve fitting method to obtain a desired smooth arc curve. A collision-free path was then determined for the leader robot from the point of departure to the end point based on the panel method. Figure 3 shows where the leader robot safely avoids the two obstacles across its trajectory.

Figure 4 shows where the streamlines around complex obstacles were calculated using the panel method to effectively determine the leader robot's collision-free path from its point of departure to the end point. Using this path, R_1, R_2, and R_3 quickly establish and maintain an ideal formation based on the leader-follower method and input-output state feedback control.

Figure 5 shows the observation angle estimation errors of the cascade multi-robot formation are also almost zero when the cascade robot formation move along the trajectory in Figs. 4., and the maximum error is 0.14 rad even when the direction changes suddenly. Figure 6 shows where the distance estimation errors of the cascade formation are also very small, with a maximum of only -0.18 m, even when the formation suddenly changes direction.

2.5 Conclusion

An autonomous navigation path for a leader robot was planned using the panel method in this study, followed by cascade multi-robot formation control via the leader-follower method. Simulation and experimental results confirm that the leader robot's collision-free path allows a cascade multi-robot formation to be rapidly established and maintained along designated streamlines.

Future research on multi-robot formation control should focus on dynamic obstacle avoidance and cascade formation transformation in complex environments to enhance the adaptability and robustness of the proposed method.

Acknowledgment

This work was supported by Natural Science Foundation of Chongqing (No. CSTB2022NSCQ-MSX1199, CSTB2025NSCQ-GPX0028), the Science and Technology Project Affiliated to the Education Department of Chongqing (No. KJZD-M202501401)，and the Science and Technology Major Project Affiliated to the Education Department of Chongqing (No. KJZD-K202201404).

References

[1] Lee, I. Service robots: a systematic literature review[J]. Electronics. 2021, 10(21), 2658.

[2] Eresen, A.N.; Imamoglu, N.; Efe, M.O. Autonomous quadrotor flight with vision-based obstacle avoidance in virtual environment[J]. Expert Systems with Applications. 2012, 39(1), 894-905.

[3] Russell-Cargill, L. M.; Craddock, B. S.; Dinsdale, R. B.; Doran, J. G.; Hunt, B. N.; Hollings, B. Using Autonomous Underwater Gliders for Geochemical Exploration Surveys[J]. The APPEA Journal, 2018, 58, 367-380.

[4] Fatma, Z.K.; Umran, O.; Pamir, K.; Ali, A.A.; Nilay, S.U.; Sercan, E.; Erdem, A. Fast Aerodynamic Analysis And Design of A Jet Aircraft by Using Panel Method[C]. 11th Ankara International Aerospace Conference Ankara, Turkey. 2021, 161-176.

[5] Merheb, A. R.; Mourad, R.; Diab, A. 3D Navigation Algorithm of a Micro-Robot Swarm in Blood Vessels for Medical Applications[J]. 2019.

[6] Yu, H.; Meier, K.; Argyle, M., Beard, R.W. Cooperative path planning for target tracking in urban environments using unmanned air and ground vehicles[J]. IEEE/ASME Trans. Mechatronics. 2015, 20, 541-552.

[7] Yi, X.; Zhu, A.; Yang, S.X.; Luo, C. A Bio-Inspired Approach to Task Assignment of Swarm Robots in 3-D Dynamic Environments[J]. IEEE Transactions on Cybernetics. 2017, 47(4), 974-983.

[8] Su, H.F.; Yang, Z.W.; Zhu, S.Y.; Chen, C.L. Bearing-Based Formation Maneuver Control of Leader-Follower Multi-Agent Systems[J]. IEEE Control Systems Letters. 2023, 7, 1554-1559.

[9] Han, Q.; Sun, S.; Lang, H. Leader-follower formation control of multi-robots based on bearing-only observations[J]. International Journal of Robotics & Automation. 2019, 34,120-129.

[10] Qing H , Hongan Y , Hao L . Bearing-Only Formation Control for Cascade Multirobots[J].Mathematical Problems in Engineering, 2016, 2016:1-13.

[11] Han Q , Sun S D , Zhi R R . Trajectory tracking cascade robot formation control[J].Control and Decision, 2016.

[12] Han Q , Wang H , Zhang C . Nonlinear controllability of leader-follower formation for multi-robots[J].IEEE, 2017.

[13] Ng K H , Yeong C F , Su E L M ,et al. Implementation of cascade control for wheeled mobile robot straight path navigation[J].IEEE, 2012.

[14] Velagi, J.; Vukovi, L.; Ibrahimovi B. Mobile Robot Motion Framework Based on Enhanced Robust Panel Method. International Journal of Control Automation and Systems. 2019, 18, 1264-1276.

[15] Belma, Ibrahimović.; Jasmin Velagić. Modified robust panel method for mobile robot path planning in partially unknown static and dynamic environments[C]. 3rd Conference on Control and Fault-Tolerant Systems (SysTol) IEEE. 2016.

[16] Du X , Ali N .Numerical Computation of Wave Forces on Blended Winged-Body Underwater Glider using Panel Method[C]. International Bhurban Conference on Applied Sciences and Technologies.IEEE, 2021.

[17] Sezer-Uzol.; Nilay.; Gazi.; Veysel.; Merheb.; Abdel-Razzak.Implementation Studies of Robot Swarm Navigation Using Potential Functions and Panel Methods[J].IEEE/ASME transactions on mechatronics: A joint publication of the IEEE Industrial Electronics Society and the ASME Dynamic Systems and Control Division, 2016, 21(5):2556-2567.

[18] Merheb, A.R.; Merheb, Y.; Atas, V.; Gazi, N.; Sezer-Uzol, N. Implementation of robot formation control and navigation using real-time panel method[C]. IEEE/RSJ International Conference on Intelligent Robots & Systems IEEE, 2010.

[19] Merheb, A. R.; Gazi, V.; Sezer-Uzol, N. Experimental Study Of Robot Formation Control And Navigation Using Potential Functions And Panel Method[C]. In joint 41st International Symposium on Robotics (ISR 2010) and the 6th German Conference on Robotics (ROBOTIK 2010), Munich, Germany, June 2010, pp. 586–593..

[20] Lu, L., Ren, H., Li, H., Zou, J., Chen, S., Liu, R. Numerical method for whipping response of ultra large container ships under asymmetric slamming in regular waves[J]. Ocean Eng. 287(2023), 115830.

[21] Panagiotou P , Dimopoulos T , Dimitriou S ,et al. Quasi-3D Aerodynamic Analysis Method for Blended-Wing-Body UAV Configurations[J]. 2021.

[22] Bilgin Z, Yavrucuk I, Bronz M. Urban Air Mobility Guidance with Panel Method: Experimental Evaluation Under Wind Disturbances[J]. Journal of Guidance, Control, and Dynamics, 2024, 47(6): 1080-1096.

[23] Katz, J.; Plotkin, A. Low Speed Aerodynamics[M]. 2nd edition, Cambridge University Press, Cambridge, UK, 2001.

[24] Lewis, R.I. Vortex Element Methods for Fluid Dynamic Analysis of Engineering Systems[M]. Cambridge University Press, Cambridge, UK, 1991.

[25] Van Nguyen, T.; Jevon, Y.; Shin, H.; Win, M.Z. Least square cooperative localization [J]. IEEE Transactions on Vehicular Technology, 2015, 64(4): 1318-1330.

[26] Wan, E.A.; Van, R.V.D. The unscented kalman filter for nonlinear estimation[C]. Adaptive Systems for Signal Processing, Communications, and Control Symposium. Lake Louise, AB, Canada. 2000, 153-158.

[27] Slotine, J.J.E.; Li, W. Applied Nonlinear Control[M]. Englewood Cliffs, NJ: Prentice-Hall. 1991, 199(1).